N63 - 18867

TECHNICAL MEMORANDUM

SELF-SEALING SPACECRAFT STRUCTURES IN THE METEOROID ENVIRONMENT

BY JAMES J. PIECHOCKI

APRIL 1963 NSL 63-64

NORTHROP SPACE LABORATORIES

1111 EAST BROADWAY, HAWTHORNE, CALIFORNIA

SELF-SEALING SPACECRAFT STRUCTURES IN THE METEOROID ENVIRONMENT

NSL 63-64
APRIL 1963

By

JAMES J. PIECHOCKI
SENIOR RESEARCH ENGINEER
SPACE MATERIALS LABORATORY

Presented at the

SECOND MANNED SPACE FLIGHT MEETING
OF THE
AMERICAN INSTITUTE OF AERONAUTICS AND ASTRONAUTICS
DALLAS, TEXAS
APRIL 1963

L. ROTH
VICE PRESIDENT AND MANAGER
RESEARCH DEPARTMENT

NORTHROP SPACE LABORATORIES
1111 EAST BROADWAY HAWTHORNE, CALIFORNIA

SELF-SEALING SPACECRAFT STRUCTURES IN THE METEOROID ENVIRONMENT

by James J. Piechocki
Senior Research Engineer
Northrop Space Laboratories

ABSTRACT

The likelihood of meteoroid encounters poses various problems to the spacecraft designer, one of them being the loss of fluids vital to mission completion. It is demonstrated that, for the more ambitious projects, a structure which provides penetration resistance only can impose weight penalties of increasing seriousness as mission times rise. Structural composites utilizing elastomeric materials reliably demonstrate in the laboratory a capability of self-sealing compatible with system requirements. In an extensive program at Northrop, and in support of a NASA-sponsored study, a variety of structural configurations successfully sealed following penetrations at speeds from 8,000 to 20,000 feet per second. The sealants are evaluated by excitation on an electrodynamic shaker, and it is shown that the more successful sealants exhibit high damping and energy dissipation when compared with the less successful materials. In a unique application of the theory of viscoelasticity, models of material response are proposed, and a qualitative description of successful operation is advanced. Material property data plus the results of hypervelocity perforations of elastomers and complete panels are presented in support of the derived conclusions.

A survey of suggested self-sealing configurations is presented. Recommendations for the practical applications of these systems are given.

1.0 INTRODUCTION

With the advent of space excursions of longer duration, the meteoroid environment must receive careful attention. No experimental data for significantly lengthy durations are as yet available to confirm the existing predictions. It is important, therefore, to assess the need for self-sealing applications and to survey the utility of these systems. As armor plate and bumper approaches have received a great amount of attention, the added or alternative benefits of self-sealing have remained hitherto unexplored. While one may recognize that self-repair concepts are not a panacea in that they do not provide for defeating penetration, it is expedient that their utility be studied. Moreover, a need to explore various sealing concepts is mandatory in view of the variety of anticipated environmental considerations and possible areas of application.

2.0 ANALYSIS OF THE REQUIREMENT FOR SELF-SEALING

2.1 The Meteoroid Environment

The presence of extra-terrestial material has been observed by man for many centuries in the manifestation of meteorites, and the threat to space travel has been discussed at great length. However, it has only been in the past decade that the hazard has been subject to quantitative scrutiny. The science of meteoroid observation has many uncertainties, and most complete evaluation will undoubtedly be gained by long-term detection satellites to realistically assess the degree of danger.

In the meantime, statistical analyses of various earth-bound observational approaches will proceed. Photographic methods seem applicable to meteor magnitudes of 6. Radio techniques extend the detection range to about magnitude 13. Some data further into the micrometeoric range have been collected by orbiting vehicles exposing relatively small areas o for limited durations.

An accurate appraisal of the environment hinges on the relation between an observed luminosity and the particle mass as it ablates in its fiery earth atmosphere entry. Some of the most reliable information of this nature was obtained in an experiment coded Trailblazer I, developed by NASA, and reported by Whipple (Ref. 1). Correlation with frequency of occurrence and meteor mass is then presented on flux versus mass charts, where the mass is presented as a threshold value. It is interesting to note the historical changes in the flux information as tabulated by various investigators. In Figure 1, it can be seen that the most current results present a somewhat more optimistic picture. The data of Whipple, presented as the 1963A line, indicates a decrease in frequency over his earlier (1957) estimate beginning from magnitude 23 and showing better than one decade decrease for magnitude 5 meteors. His conclusion tends toward the 1956 results of Watson[2]. Indeed, an alteration in the mass-magnitude relation reflects this change.

Meteoroid size can only be determined from mass and density relations, both of which are speculative. However, there is general agreement among investigators that the prime hazard is due to the micro-sized debris, or micrometeorites.

The flux data can be converted into an index of the penetration hazard. This is done by converting the meteor mass to an equivalent wall thickness penetrated by it, assuming values for the meteor parameters of velocity and density, and a pertinent penetration equation. The reciprocal flux plotted versus the threshold wall thickness defines an average time to penetration of a unit area for any selected group material. The assumed values of the attendant parameters are:

(a) Average meteoroid density, $\rho = 0.44$ gm/cm^3

(b) Average meteoroid velocity, $V = 22$ km/sec

(c) Herrmann - Jones thick target penetration formula (Ref. 3):

$$P = 0.6\left(\frac{6}{\pi}\right)^{\frac{1}{3}} \frac{\rho^{1/3}}{\rho_t^{2/3}} \ln\left[1 + \left(\frac{\rho}{\rho_t}\right)^{2/3} \frac{\rho_t V^2}{4H}\right] m^{1/3}$$

with p = thick-target depth of penetration
ρ_t = target density
H = target Brinnel hardness
m = meteoroid mass

(d) Thick target penetration depth = 2/3 thin sheet penetration depth

The relatively low meteoroid density is proposed in Reference 1, and is consistent with the generally accepted notion of the cometary origin of over 90 percent of the debris (Ref. 4). Whipple also accepts the listed penetration relation as applicable for low density particles.

The average-time-to-penetration data is shown in Figure 2 for the two sets of Whipple data, viz., that of 1957 and 1963 estimates. It can be seen that for a 0.1 cm skin thickness (about 0.040-inch) the penetration time has been increased by a factor of over 3,000. This result accrued with an intended pessimism of one order of magnitude in the 1957 data. The changes in the data over six years of effort arise from the alterations in the flux information and the penetration relation and criterion.

Future changes in the penetration equations are not expected to be drastic, although laboratory projection techniques for realistic speeds and particle masses still require development. Uncertainties in the density estimates could reduce the average time to penetration by one order of magnitude below the "best estimate." According to Figure 3, a vehicle of 1,000 ft^2 exposed surface (about 90 $meters^2$) with an aluminum skin thickness of 40 mils designed to a realistic zero penetration probability could be penetrated in less than one month. The problem increases linearly with larger vehicle size.

The need for meteoroid protection for extended missions is obvious, as is the existence of a variety of uncertainties in its implementation for the shorter ones. Long-time orbiting detectors will provide better data for a realistic assessment of probabilistic vehicle design, but the time to implement these efforts must not inhibit current or future development. The biomedical results of a penetration-induced decompression have been detailed elsewhere, and will not be discussed here. However, it has been reliably stated that incapacitation of an exposed biospecimen could result in seconds.[5] Self-sealing systems, with nearly instantaneous response and no extraneous crew monitoring, are logically suggested. Hence, for unmanned compartments, for inaccessible areas of the vehicle, and even as a complement to armor plate, self-sealing structures "design around" the environmental problem and present a greater degree of crew comfort and safety.

2.2 System Comparative Evaluation

One method of observing the utility of self-sealing is to compare the expected weights of various systems for different mission times. Such an analysis has been made for the following systems employing aluminum skins:

(a) An air replenishment system with provisions for maintaining a 14.7 psi air atmosphere with no provisions for repair.

(b) An armor plate structure with a zero penetration probability P(o), of 0.99.

(c) A self-sealing structural composite.

The Whipple 1963A "best estimate" flux data was assumed. The air replenishment system is assumed to have the capacity to replace air at a rate necessary to maintain the specified pressure to offset the predicted loss from hole production flux, with an equipment weight penalty of 40 percent of the lost mass[6]. Ideal nozzle flow was assumed in calculating the mass loss. The armor plate concept is applied to a vehicle of 1,000 ft^2 of exposed surface area. The penetration relationship selected for ease of computation is that of Rodriquez[7], which is a generalized form of that of Kornhauser[8].

The self-sealing systems employ an elastomeric sealant confined in a honeycomb core sandwich, and will be described in detail later. Successful laboratory specimens of this type have been fabricated with a unit weight of 1.7 lb/ft^2 (not including the metallic face). This current optimum has been used for the weight analysis.

An average meteoroid velocity and density of 22 km/sec and 0.44 gm/cm^3, respectively, taken from Whipple, are assumed. The complete analysis is shown in Figure 3. The air replenishment concept becomes noncompetitive at mission times beyond one month. For times greater than two weeks, the 0.100-inch system is actually lighter than its companion 0.020-inch skin system since only the less frequent, more massive, perforations are experienced. A comparison of armor plate and self-sealing yields interesting results. For the range of sealant constructions between 0.020-inch and 0.100-inch aluminum face thicknesses, a weight advantage over armor plate is predicted for mission times beyond two days to about two weeks. Moreover, the 0.020-inch air replenishment concept would still be lighter up to about two weeks.

It becomes apparent that the weight tradeoff point for self-sealing configuration occurs for mission times beyond two weeks. Hence, for near-earth performance, vehicles could utilize these structures to a weight advantage assuming that the particle flux rate is not significantly altered. As discussed earlier, the flux data are considered to be reliable to the extent that any future revisions should not produce drastic changes. Some further optimizations in the self-sealing geometries can be expected, but their effect should not be drastic either. Hence, the weight picture of armor versus self-sealing as presented here is considered quite realistic.

The "bumper" concept has not been analyzed here because of the scarcity of data at this time. It can be reasonably expected that considerable weight saving can be effected if one were to apply the laboratory optimums.[9] Indeed, factors of 50 percent and higher have been reported. However, it is interesting to note that these optimums occur at geometries where a considerable percentage of the total penetrated depth (bumper plus witness plate) is in the rear wall. This situation may be intolerable for cryogenic tankage where the residual energy of penetration (past the bumper) may be severe enough to initiate shock effects in the confined fluid. Applying this further to manned capsules,

one need be concerned about structural wall crack formation with or without a bumper, since a penetration-resistant structure may not necessarily be leak-proof. However, nonoptimum bumpers may be employed. For this reason, a factor of 30 percent weight savings may be a more realistic assessment of bumper efficiency. With this factor applied directly to the armor plate curve of Figure 3, the weight tradeoff for bumper versus self-sealing occurs between ten days and three months for self-sealing configurations using aluminum skins of 0.020-inch to 0.100-inch thickness for the structural requirement.

3.0 SEALANT MATERIAL REQUIREMENTS

Depending on the area of application, self-sealing materials must satisfy specific requirements. Many of these demands are obvious and are listed as follows:

- Minimum permanent deformation following hypervelocity perforation coupled with good recovery characteristics.
- Sufficient strength and crack propagation resistance under extremely rapid loading to localize damage and material removal.
- High internal loss characteristics to facilitate energy dissipation.
- Resistance to degradation by the induced environment.
- Chemical properties compatible with fire resistance, permeability, and minimal odor and toxicity of the degradation products.

Bjork[10] describes the process of hypervelocity penetration as a fluid phenomenon, neglecting the inherent strength of the material, and considering it equivalent to the propagation of a pressure wave in the megabar range. Eichelberger and Gehring[11] have further postulated that the hydrodynamic analogy yields accurate predictions for the initial stages of crater formation, and that descriptions of the final stages must account for the mechanical after-flow of the impacted material. Charters[12], in describing crater formation, refers to a rebound or recovery of 15 percent of the maximum formed crater volume in the final stage of penetration.

These descriptions were made from observations of impacts on thick metallic targets. However, many aspects of the penetration mechanism apply equally well to the elastomers. It is this inherent ability for recovery from as much as 100 percent strain which renders the elastomers applicable to self-sealant usage. Figures 4 and 5 show the entry and exit face, respectively, of a penetrated panel. The remarkable degree of recovery is evident in both photos of this penetration which occurred at approximately 7,000 feet per second. The tendency of elastomers to exhibit viscous responses further serves to enhance their application in view of the attendant energy dissipation to be expected. The notion of a sealing mechanism utilizing a flow process is a feasible (as well as aesthetic) possibility and will be described later.

These salient requirements, along with compatibility with the structural function of the shell, made the elastomers a logical class of materials for this purpose. The use of the elastomers for static seals is well known and prevalent. The further possibility of tailoring the material to specific requirements is available to a high degree in view of the presence of this effort in polymer research.

4.0 SURVEY OF SELF-SEALING CONCEPTS

All of the concepts discussed here were initially subjected to perforations at 7,000 to 8,000 fps. Lead, steel, and glass projectiles of 1/8-inch diameter were used. The particle accelerator range was evacuated to approximately 200 microns for each shot. The exit side of the specimens were exposed to ambient conditions, so that sealing was being observed across essentially a 14.7 psi pressure differential. Immediately after firing, sealing was qualitatively checked by ear and with the assistance of a stethoscope placed onto the exit side near the perforation. Following this, leakage rates from a known volume container over a spectrum of pressure differentials were measured using laboratory-type flowmeters. Further testing of the more promising configurations was then conducted at hypervelocity facilities at velocities in excess of 20,000 fps.

4.1 The Honeycomb-Core Sealant Concept

The basic configuration is shown in Figure 6. It consists of a metallic face sheet and a reinforced neoprene backstrip confining a phenolic fiberglass honeycomb core. The core is filled with the sealant and proper surface treatments are used to insure good sealant-to-core and -face bonding.

A rubber backup strip, with a good bond to the core-sealant, seems to be a necessity. Early experiments which included shots into panels with metallic rear faces exhibited severe damage on the pellet exit side (see Figure 5). In most cases, sealant material local to this area was also observed to be severely damaged and hole closure was not achieved. When neoprene was substituted, immediate improvement was observed in the form of decreased deformation of the backup sheet and adjacent sealant. Since the area bounded by the backup strip represents a free surface with expected shock wave reinforcement due to reflection, it is apparent that a dissipative material is required. The resiliency of the neoprene further permits recovery from radial deformations due to the passage of the particle, and enhances hole closure.

The function of the honeycomb core is to contain the sealant and provide damage confinement through the addition of bonding surfaces in the sealant volume. However, aluminum honeycomb geometries exhibited massive damage. Radial collapse of the cell walls as much as twelve times the projectile diameter, with attendant sealant damage, was observed. Again, the need for a more dissipative material was apparent. The use of phenolic fiberglass core, with attention to maintaining good core-to-sealant bonding, was seen to greatly alleviate the damage. Subsequent firings resulted in little or no core damage and localization was achieved.

Sealant materials used in the initial work were commercially available silicones, polysulfides, and polyurethanes. The silicones were observed to exhibit minute radial cracking local to the particle path and did not seal with the reliability of the latter materials. The polysulfides and polyurethanes used successfully can best be described as less viscous and, hence, more amenable to creep or flow characteristics which are obvious from static handling of the materials. It was these observations which suggested a method of dynamic material testing and evaluation, to be described later in this paper.

A highly successful configuration consists of a 0.020-inch aluminum face, 3/16-inch thick core, with 3/16 or 1/4-inch cells filled with a polysulfide elastomer, and a 1/16-inch fiber-reinforced neoprene backup sheet. The self-sealing weight contribution is 1.7 pounds per square foot, and the over-all weight is approximately 2.0 pounds per square foot. Best results are observed when the bonding agents used are the same material as that of the sealant. Since all tests were conducted with 1/8-inch diameter projectiles, it is conceivable that some further weight reduction may be achieved with more realistic (vis., smaller) projectile sizes.

To further observe isolated sealant response to dynamic puncturing, various configurations were penetrated. These consisted of shots into 1/4-inch and 1/2-inch discs of sealant material in variously supported geometries. Shots were made into various permutations with and without face sheets and backup sheets. Where possible, a circular grid was molded onto the surface of the sealant disc, and both pre- and post shot spacings of the grid lines were made. In some cases, residual radial surface strains adjacent to the entry crater were observed to be tensile. For the majority of cases, residual strains were found to be undetectable or below 3 percent, indicating that the specimen surface was relatively undamaged. Upon dissection of the specimens, inspection of the damage at the particle path revealed local tearing in a direction opposite to the direction of the projectile. Delamination in the radial direction extending out from the particle path was indicative of the presence of localized shearing through the specimen thickness. The deposition of material toward the hole in both instances just discussed is considered desirable, in that both surface and subsurface inward displacement of the sealant minimize hole size and, hence, leakage rates.

Figure 7 shows a typical surface damage in what is considered a brittle silicone rubber. Figure 8 shows the identical situation for a highly successful polysulfide sealant. The cross-sectional view of a perforation in a 1/4-inch silicone rubber is shown in Figure 9. The displacement of the material back along the pellet direction cannot be explained in terms of wave theory. One simple explanation is that the short-duration heat pulse upon puncturing melts the surrounding material, and the subsequent air flow across the slab initially forces material back along the particle path. In any event, this displacement of the material back into the hole assists the sealing process.

An example of successful self-sealing following a 20,000 fps penetration in the mechanical configuration is shown in Figure 10. The backup sheet has been pulled back to show the localized interior damage. In every instance shown, the sealant material is seen to be deposited in the entrant hole, and the exit damage is quite remarkably localized.

Residual leakage rates for the successful panels were measured by observing the pressure drop from a known volume container capped with the penetrated specimens. Leakage rates as low as 2.0 lb/yr to zero have been observed. Average leakage rates have been found to be on the order of 1 to 2 lbs/day, which is an improvement of better than 99 percent over the observed rates through the penetrated aluminum face sheet hole. In many instances, the specimens showed a detectable leakage rate across a 14.7 psi pressure differential, but exhibited almost complete sealing at 4 to 5 psi internal pressures.

4.2 Elastomeric Sphere Concept

The concept just described relies on both the energy dissipation and the recovery of the sealant material for successful operation. For extremely localized damage, the recovery of the material in the domain of infinitesimal deformations is utilized to effect hole closure. It is conceivable that under certain environmental conditions and with massive face sheet and sealant damage or tear-out, macro-motion of the sealant into the perforated zone will be required. For this reason, the elastomeric sphere concept was investigated. Here, the conventional sealant is replaced by discreet elastomeric spheres to a predetermined packing density (see Figure 11).

Upon penetration, the pressure differential between the inside cabin and the vacuum of space forces the balls toward the entrant hole and effects the sealing. Ball size, packing density, and material will control the mobility of the spheres and the sealability. This concept exhibited residual leakage rates that are comparable with the mechanical system described earlier, and is currently under further study.

4.3 Other Systems

A number of alternate concepts developed to fit a variety of requirements have been successfully tested. They may be classed as mechanical or chemical depending on the mode of activating the sealing process.

One highly successful approach is to prestress the sealant in compression. This enhances the sealability of materials which have desirable thermal or vacuum properties, but which exhibit brittle-type fractures or low shear strength characteristics under dynamic conditions when simply confined. The relatively low modulus characteristics of the elastomers facilitate the buildup of moderate internal stresses with appreciable strain recovery in the penetration hole. The prestressing can be accomplished in a variety of simple and ingenious ways.

One prestressing technique uses an elastomer and foaming reagent which causes an unconfined volume expansion of 200 percent to 300 percent upon curing. The structural panel is filled with the uncured sealant compound to a volume fraction which will produce a desired prestress level. Face plate bonding is accomplished with a material whose softening point is above the cure temperature of the sealant. The sealant is then cured at the required heat. This technique has shown successful sealing characteristics with a high degree of reliability.

Chemical concepts rely on the dynamic action of the penetrating particle to initiate a reaction which closes the hole. In one concept, shown in Figure 12, an uncured polymer is separated from the catalyst by a thin, nonreactive membrane. Upon complete perforation, the pressure differential across the panel forces a mixture of polymer and catalyst through the hole. Very fast curing mixtures have been used with complete and repeatable sealing action. In another method, small bags of catalyst are interspersed in the sealant void (see Figure 13). This seems to localize the curing action to the area of the penetration. Bag size is an important factor in this method. For very uniform distribution of the catalyst in the uncured elastomer, microencapsulation techniques can be adopted.

In all of the chemical concepts where the sealant materials are initially fluid, careful attention must be given to the rheological or flow properties of the polymer. The viscosity of the material must be such as to permit an initial gradual flow through the hole without excessive loss. Cure rate must obviously be rapid enough to "set up" the material in the hole. Environmental stability must be carefully considered against mission time, as degradation can severely alter flow rates and, hence, sealability.

5.0 SEALANT MATERIAL EVALUATION

Observations of a variety of sealing results following perforation indicate the importance of the proper selection of the sealant material. Indeed, material differences are apparent from static handling of the specimen material. The highly elastic or rubbery materials tested exhibit a tendency toward crack formation and excessive volume removal or tear-out. When a less viscous material was substituted, immediate improvement was noted. This improvement is characterized by a remarkable degree of damage localization in the form of a minute particle path with little or no surface damage. Unfortunately, such terms as "less viscous" or "more elastic" are purely relative and do not assist in a quantitative description of material response. One method of assessing the use of a solid elastomer may be derived from a consideration of the theoretical response of viscoelastic materials.

5.1 Theoretical Material Response

Ideally, viscoelastic materials are assumed to consist of elements whose over-all behavior can be described as a combination of viscous and elastic responses. Ideal springs and Newtonian viscosity characterize linear behavior and permit the use of the principle of superposition.

Some classical bodies are shown in Figure 14 along with their stress-strain equations. Most real elastomers depart from this ideal behavior, exhibiting a spectrum of retardation times which makes difficult a complete description of response over a broad range of loading rates or frequencies. However, responses over a selected frequency bandwidth, specified by design criteria, can be accomplished. A response fit over a decade of frequency is considered adequate.

The most general characterization of a material with a time response in shear can be written as (Ref. 13):

$$P\{S_{ij}\} = 2Q\{E_{ij}\}$$

where Sij and Eij are the deviatoric stress and strain tensors, respectively, and P and Q are differential operators whose coefficients define material properties. A Laplace or Fourier mathematical transform may be performed which alters the time-dependency to one of frequency. The notion of modulus is retained in the form

$$\frac{\bar{Q}}{\bar{P}} = E' + iE''$$

denoting the complex modulus, with barred quantities denoting transformed properties. Since the value is complex, it denotes in a vector representation in-phase and out-of-phase components. The in-phase component is referred to as the elastic or storage modulus; the out-of-phase component is called the loss modulus. For low to moderate damping ($E''/E' < 0.2$), it can be shown that the ratio of E''/E', or loss factor, is a measure of the percent energy dissipation of the material (Ref. 13).

Sinusoidal excitation may be performed by a variety of means which include the vibrating reed or rocking beam. The intent at this point is to simulate the loading rate of hypervelocity perforation. This implies that excitation be performed in the kilocycle range. However, power limitations severely hamper the generation of detectable mechanical displacements at those extremely high frequencies. For this reason, correlation with theoretical models of material response was attempted at moderate frequencies from 100 to 2,000 cps in an attempt to describe successful self-sealing operation of solid elastomers at impact speeds of 5,000 to 7,000 feet per second.

5.2 Results of Dynamic Excitation

The oscillatory test method employs a three-inch diameter, 1/4-inch thick elastomer specimen, with a mass bonded to its upper surface. The elastomer-mass combination is bonded to a rigid mounting plate, which is in turn attached to the head of a conventional electrodynamic shaker. Bonding agents used were the same material as that of the specimen to insure homogeneity. The test geometry is shown in Figure 15. Input and output accelerometers, along with the associated phase angle were recorded for fixed output "g" levels to maintain constant peak stress on the sealant over the frequency range tested.

Considerable in-plane restraint was evident on the specimen, resulting in an apparent stiffening of the material. However, it was felt that this geometry most nearly simulated the confined sealant in a panel configuration. Two silicone rubbers, which exhibited poor to inconsistent self-sealing, and a polysulfide and a polyurethane elastomer with superior performance, were the four materials selected for initial evaluation.

The results of the oscillatory tests are shown in Figures 16 and 17. The in-phase or elastic modulus results indicated that the two successful self-sealants exhibited higher in-phase or recovery moduli. From Figure 17, it is seen that the energy dissipation characteristics of the polysulfide and polyurethane materials were superior at the higher frequencies. It is concluded that the extremely high damping capability of the latter two materials at the higher frequencies renders them more suitable for this application.

It is to be noted that the in-phase or elastic moduli values of Figure 16 are considerably higher than Young's modulus information reported in the literature. Owing to the test geometry which imposes radial restraint on the specimen due to the bonded surfaces and the short specimen height, the results are more closely in agreement with bulk modulus. For a purely elastic, isotropic material with complete lateral restraint, normal deformations are volumetric, and the associated stiffness is the bulk modulus, K, where

$$K = \frac{E}{3(1-2\nu)}$$

and ν is Poisson's ratio. An incompressible material (ν=0.5) has an infinite bulk modulus. Furthermore, pure volumetric deformations are minimized with increasing bulk stiffness. Obviously, complete recovery ameliorates the self-sealing situation by effecting hole closure following perforation. Naturally, maximum closure, and hence, minimum leakage would result with minimum material loss or tear-out. Consequently, high internal dissipation in shear from a controlled viscosity is consistent with minimizing material loss. A sealant material rigidly confined, having a relatively high bulk modulus and internal dissipation is adjudged superior.

Another method of material evaluation used is the standard Lupke resiliency test. In this test, a specimen of the candidate material is impacted by a pendulum and the degree of successive rebounds is recorded. Although this test provides relative information only, it has been highly useful for initial screening of materials for energy absorption capability.

6.0 CONCLUSIONS AND RECOMMENDATIONS

The need for self-sealing structural systems has been described in view of the many uncertainties in the meteoroid environment assessment. Moreover, these uncertainties are expected to be present for a number of years to come. Practical self-sealing composites have been developed in the laboratory which provide a greater degree of safety with the added feature of self-repair to minimize crew responsibility. Hole closure can be accomplished either mechanically by utilizing the inherent ability of the elastomers to recover deformations, or chemically by employing a mechanism actuated by the penetrating particle. Weight considerations appear attractive for the longer missions, where the term "longer" applies by present calculations to missions of a duration beyond two to four weeks. The need is even more urgent if one considers that penetration-resistant structures may not necessarily be completely leakproof following a meteoroidal collision.

Material behavior under the space environment must be carefully assessed, and stable materials are mandatory. Both mechanical and chemical methods have been shown to be practical when careful attention is given to material bulk and compressibility properties, and that of flow. The combined attention of the structural designer and the chemist has been a necessity in the development of the current concepts.

A qualitative description of the mechanical self-sealing mechanism has been forwarded based on the measurement of aggregate material dynamic properties. A complete theoretical analysis would be beneficial, but is beset with the vagaries also associated with the thick-target hypervelocity penetration problem.

As self-sealing structures are not specifically intended to defeat the incoming meteoroid, their area of application may seem to be restricted. However, as a complementary system for either armor plate or bumper constructions, a significant increase in safety can be expected. Use of elastomers as a back-spall preventative appears possible, but requires further study.

Greater usage can be expected in areas of the vehicle having a minimum of personnel activity (e.g., passageways, airlocks, etc....). Tankage protection is another area where the dissipative capabilities of elastomers may prove feasible, with uniquely designed self-sealing systems employing tailored materials.

ACKNOWLEDGMENT

The author wishes to express his thanks for the valuable assistance in the preparation of this paper of his co-workers of the Space Materials Laboratory, Northrop Space Laboratories, R. D. Johnson, Head. The majority of the results presented were obtained under NASA contract, NASr-102, "Self-Sealing Structures For The Control of the Meteoroid Hazard to Space Vehicles," N. G. Mayer, Project Monitor of NASA Headquarters.

REFERENCES

1. Whipple, F. L., "On Meteoroids and Penetration", paper presented at Ninth Annual American Astronautical Society Meeting, Los Angeles, California, January, 1963.

2. Watson, F. G., "Between The Planets", Harvard University Press, Cambridge, Massachusetts, 1956.

3. Herrmann, W., and Jones, A. H., "Correlation of Hypervelocity Impact Data", Proc. 5th Symposium on Hypervelocity Impact by the Tri-Service

Committee, April, 1962, Vol. I, Part 2, pp. 389-438.

4. Hawkins, C. S., and Southworth, R. B., "The Statistics of Meteors in the Earth's Atmosphere", Smithsonian Contributions to Astrophysics, Vol. 2, No. 11, Smithsonion Institution, Washington, D. C., 1958.

5. Konecci, E. B., "Decompression Events In Biosatellites", ARS 638-58, presented at the Semi-Annual Meeting of the ARS, Los Angeles, California, June, 1958.

6. Carter, J. W., and Bogeman, B. L., "Inflatable Manned Orbital Vehicles", Proc. of the Manned Space Station Symposium, Los Angeles, California, April, 1960.

7. Rodriquez, D., "Meteoroid Shielding For Space Vehicles", Aerospace Engineering, Vol. 19, No. 12, December, 1960.

8. Kornhauser, M., "Prediction of Cratering By Meteoroid Impacts", Advances In Astronautical Sciences, (Proc. of Fourth Annual Meeting of AAS, December, 1957; Plenum Press, Inc., New York, 1958.

9. Wallace, R. R., Jr., Vinson, J. R., and Kornhauser, M., "Effects of Hypervelocity Particles on Shielded Structures", ARS 1683-61.

10. Bjork, R. L., "Effects of Meteoroid Impact on Steel and Aluminum in Space", Proc. of Tenth International Astronautical Congress (London 1959), Wien-Springer-Verlag, 1960.

11. Eichelberger, R. J., and Gehring, J. W., "Effects of Meteoroid Impacts on Space Vehicles", ARS 2030-61.

12. Charters, A. C., "High Speed Impact", Scientific American, Vol. 203, No. 4, October, 1960, pp. 128-140.

13. Alfrey, T., Jr., "Mechanical Behavior of High Polymers", Vol. VI, High Polymers, Interscience Publishers, Inc., New York, 1948.

14. Kornhauser, M., "Current Estimates of the Effects of Meteoroids on the Skin of a Satellite Vehicle", ASVE Memo No. 3, Missile and Space Department, General Electric Co., 25 Feb. 1960.

15. Hughes, R. F., "Meteoroid Impacts and Their Effects on Ballistic Missiles", Real Gas Tech. Memo #13, 23 July 1956.

16. Whipple, F. L., "The Meteoric Risk to Space Vehicles", Vistas in Astronautics, pp. 115-124, Pergamon Press, New York, 1958.

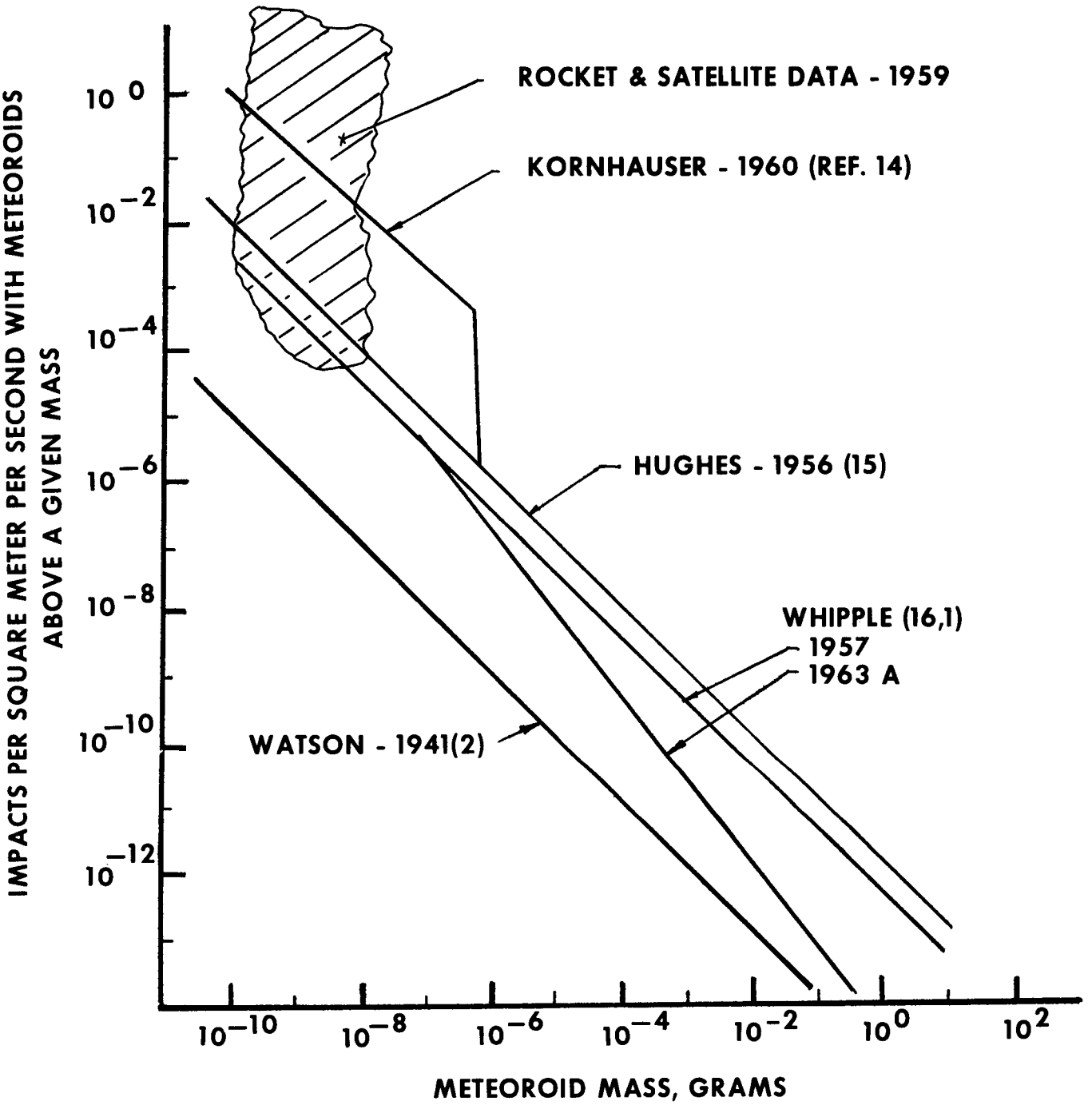

FIGURE 1 METEOROID FLUX ESTIMATES

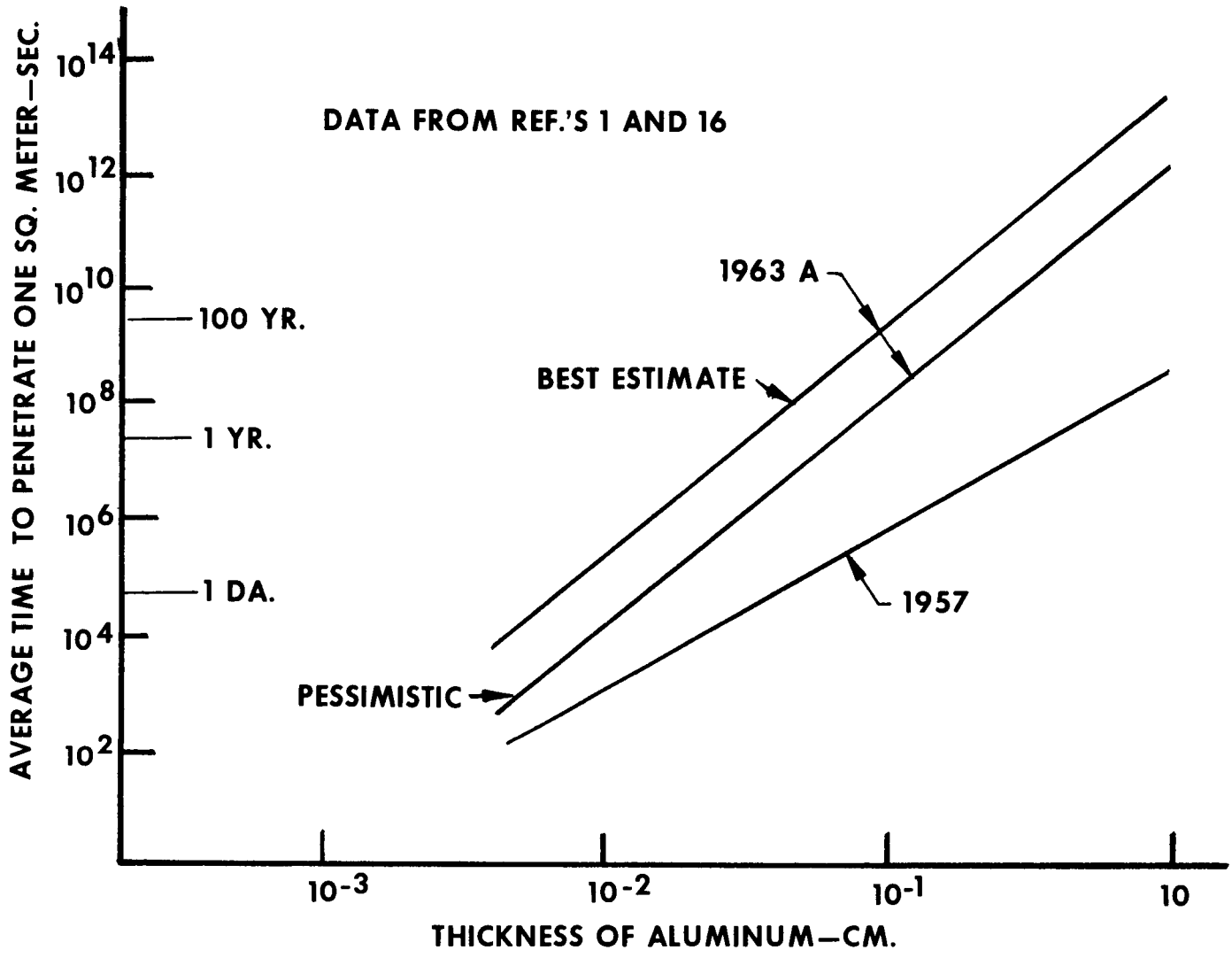

FIGURE 2 WHIPPLE ESTIMATES OF THIN-SKIN PERFORATION

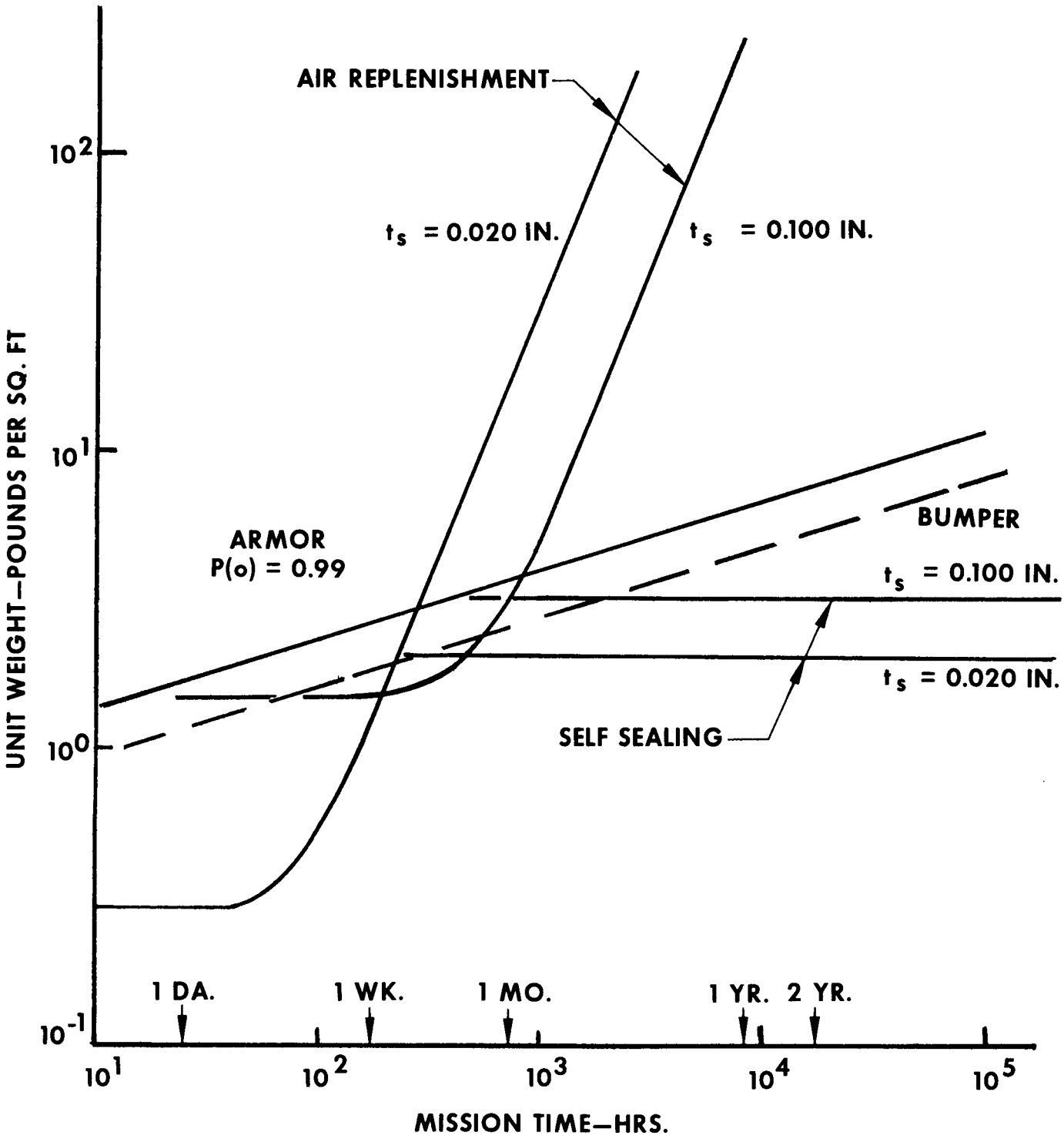

FIGURE 3 SYSTEM WEIGHT COMPARISON

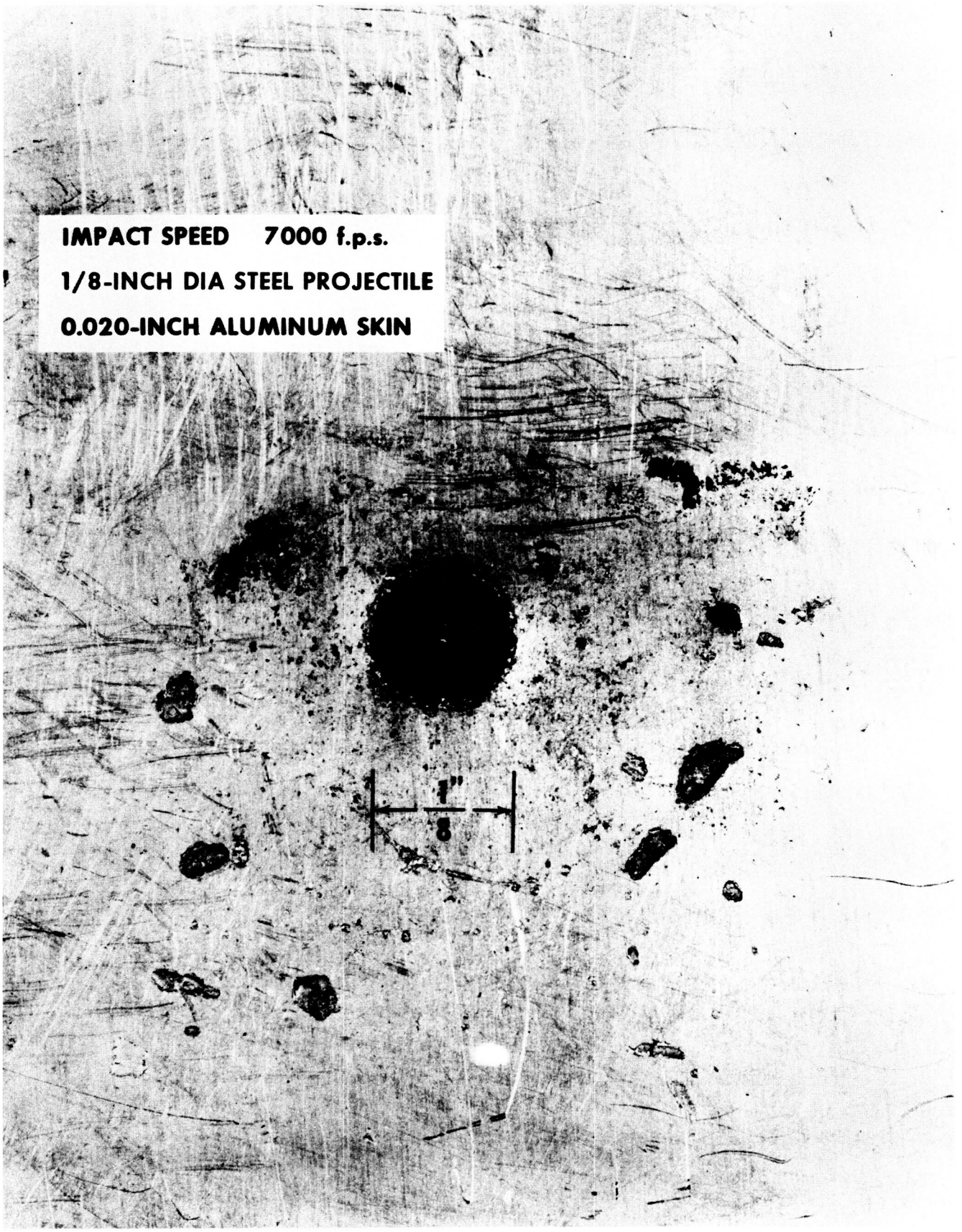

FIGURE 4 ENTRY DAMAGE TO SELF-SEALING PANEL

FIGURE 5 EXIT DAMAGE TO ALUMINUM REAR WALL

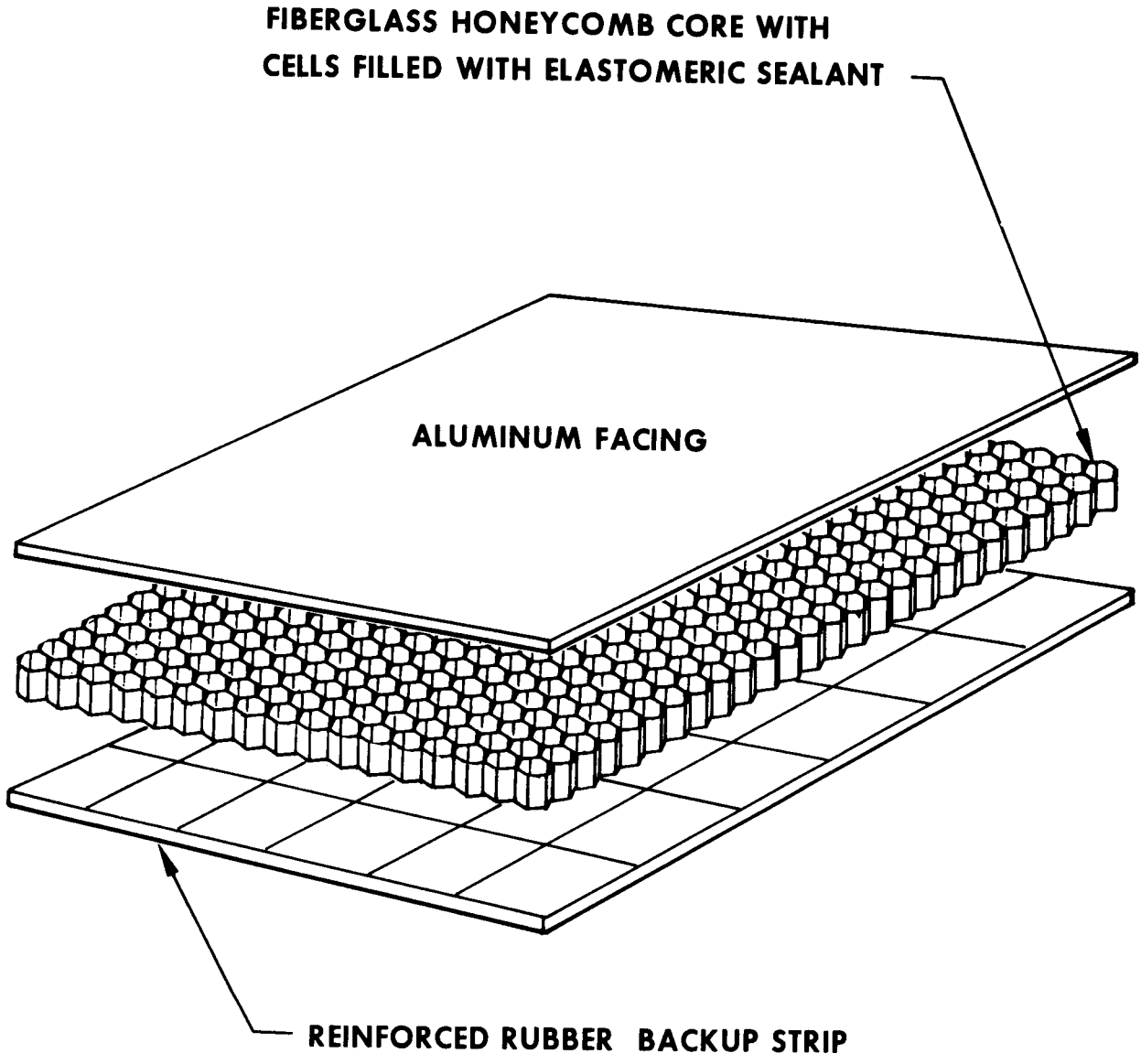

FIGURE 6 BASIC HONEYCOMB CORE
SELF-SEALING CONCEPT

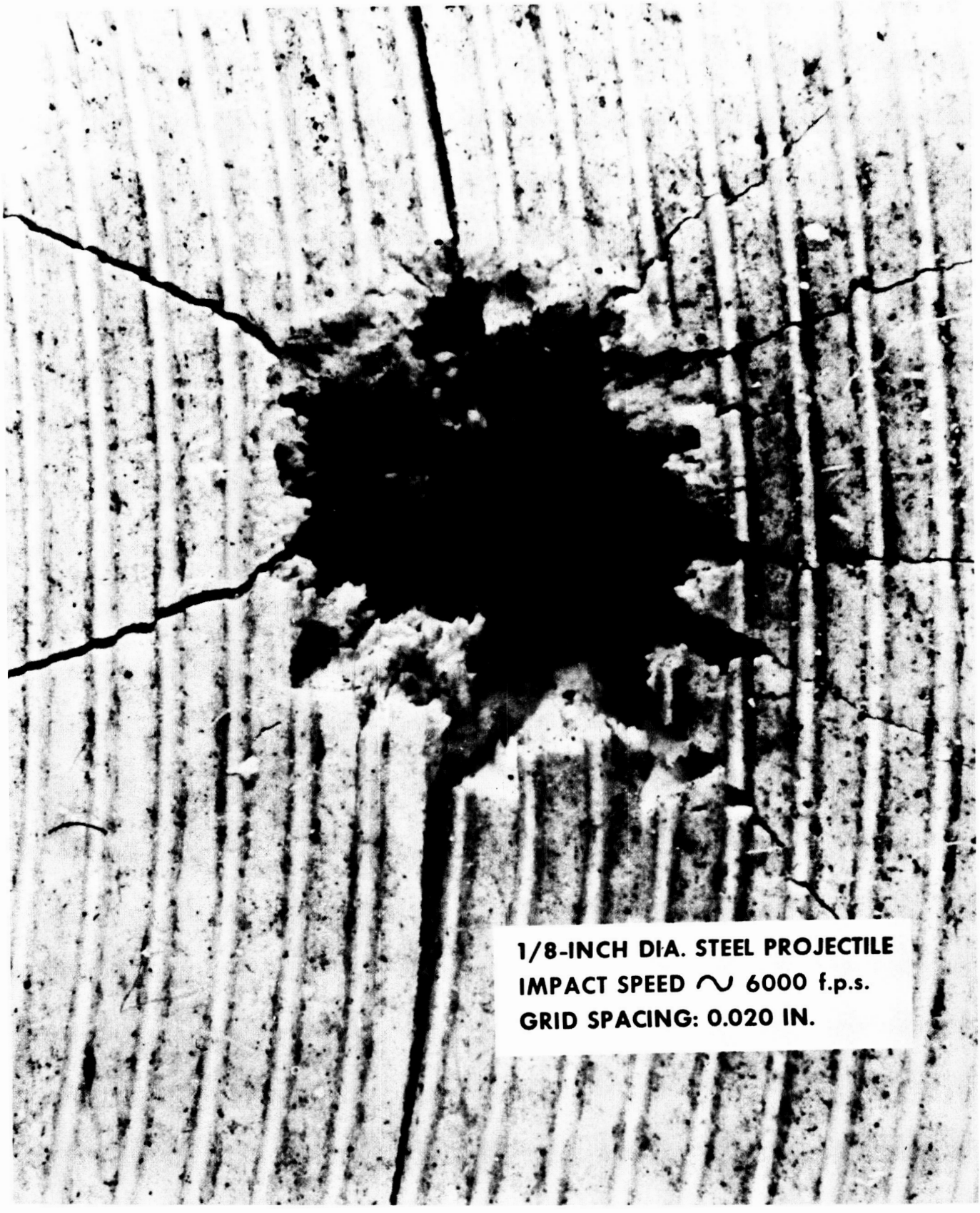

FIGURE 7 ENTRY DAMAGE TO SILICONE RUBBER SPECIMEN

FIGURE 8 ENTRY DAMAGE TO POLYSULFIDE ELASTOMER SPECIMEN

FIGURE 9 PERFORATION DAMAGE TO
½-INCH THICK SILICONE ELASTOMER

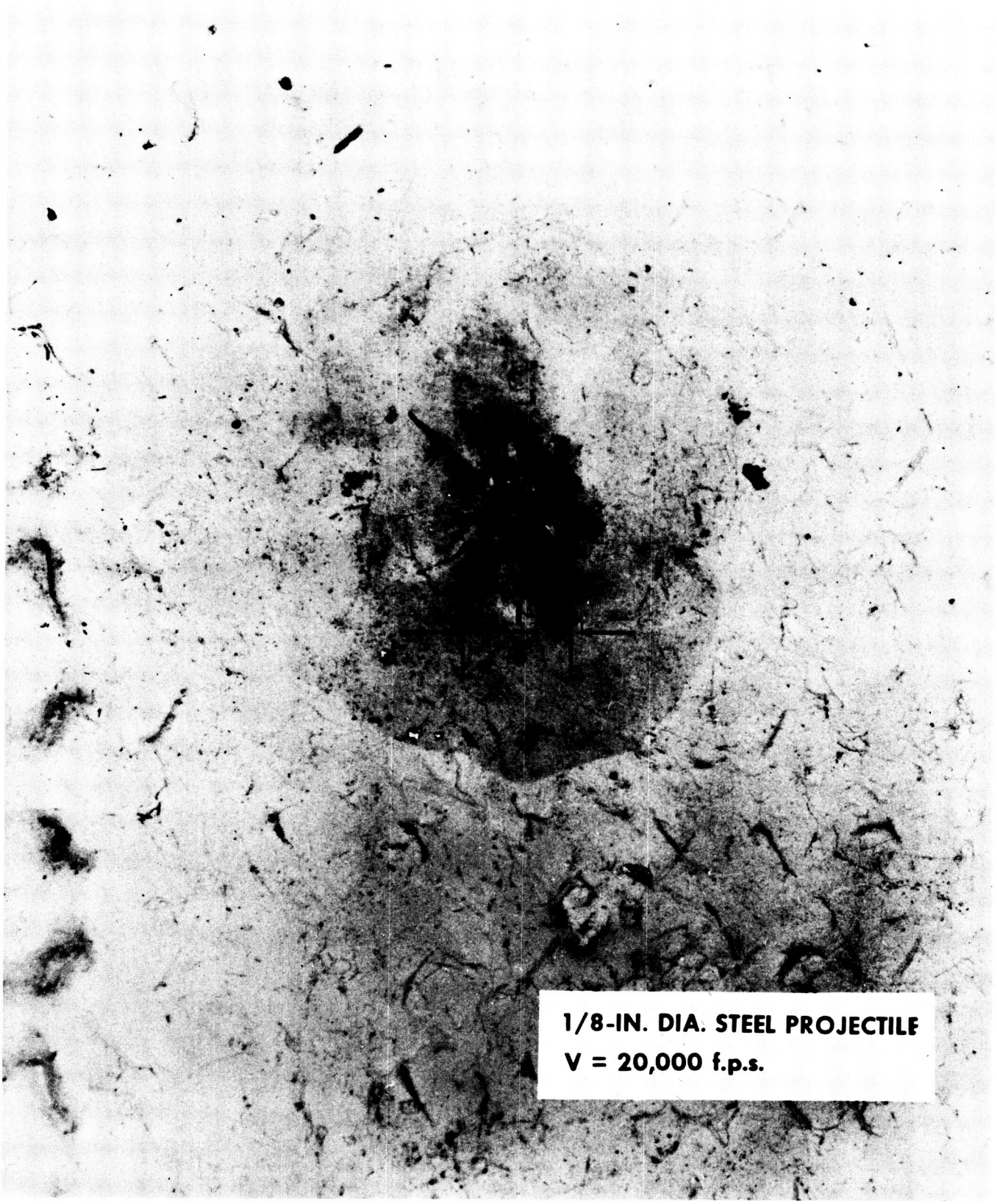

FIGURE 10 SEALANT EXIT DAMAGE
IN HONEYCOMB-CORE PANEL

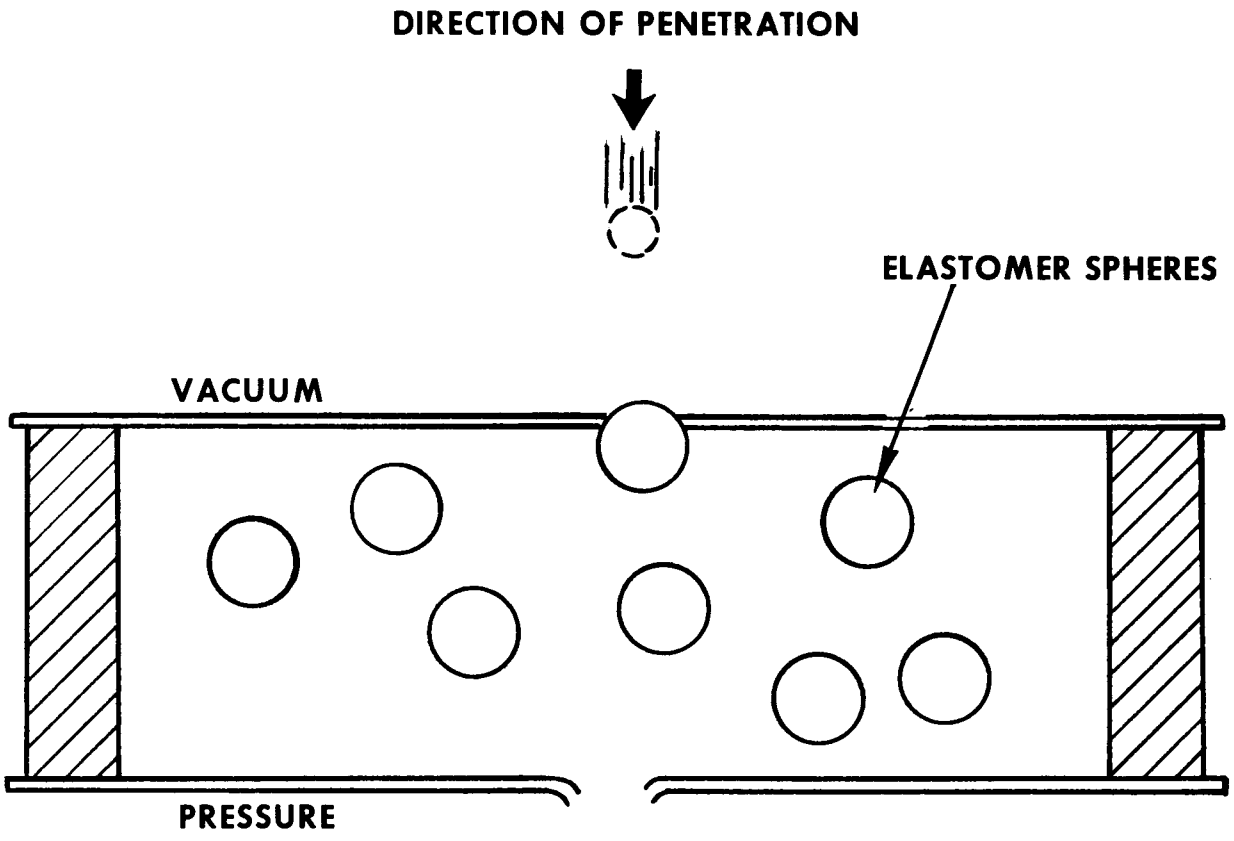

FIGURE 11 ELASTOMERIC SPHERES SELF-SEALING CONCEPT

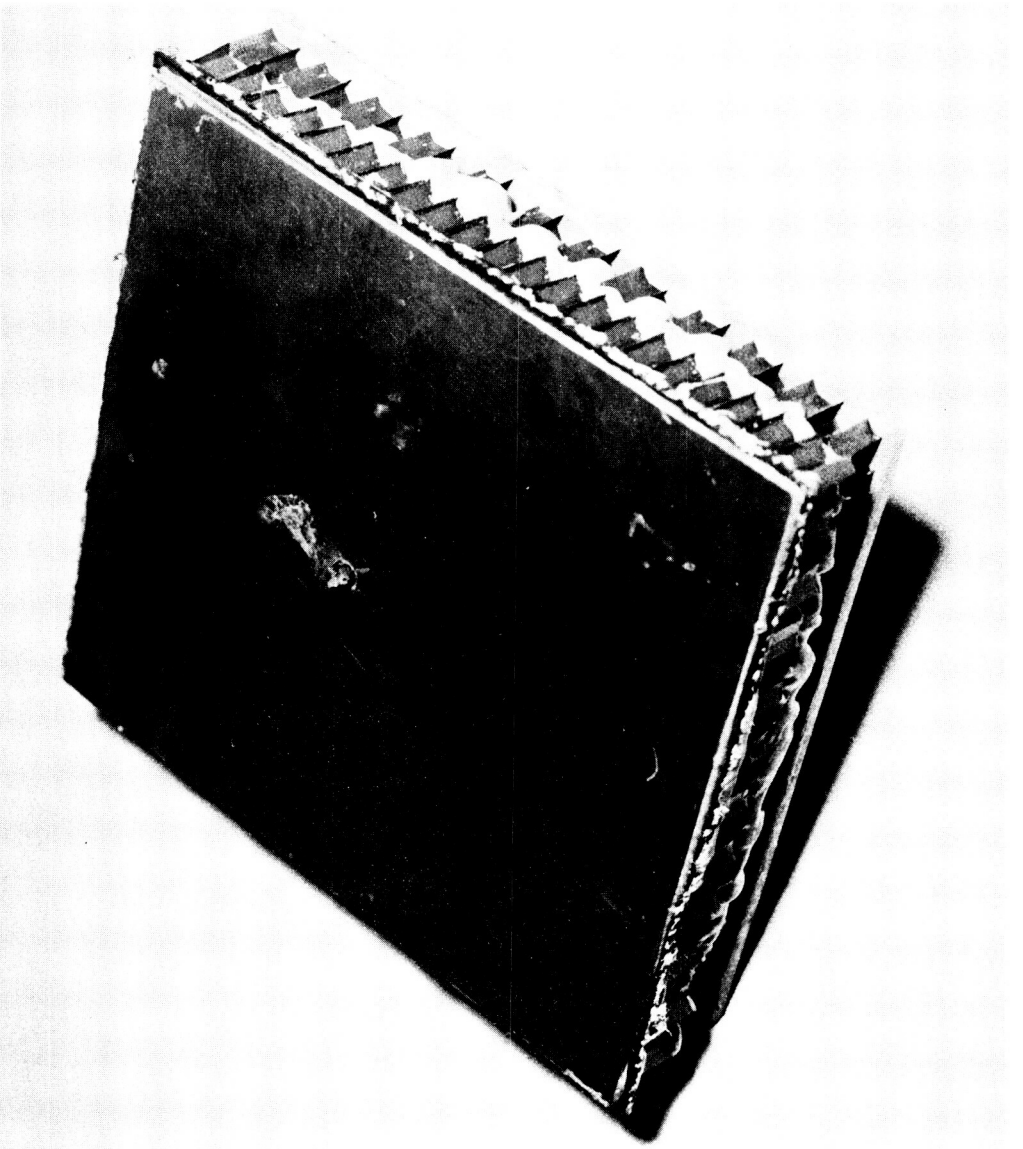

FIGURE 12 CHEMICAL MEMBRANE CONCEPT

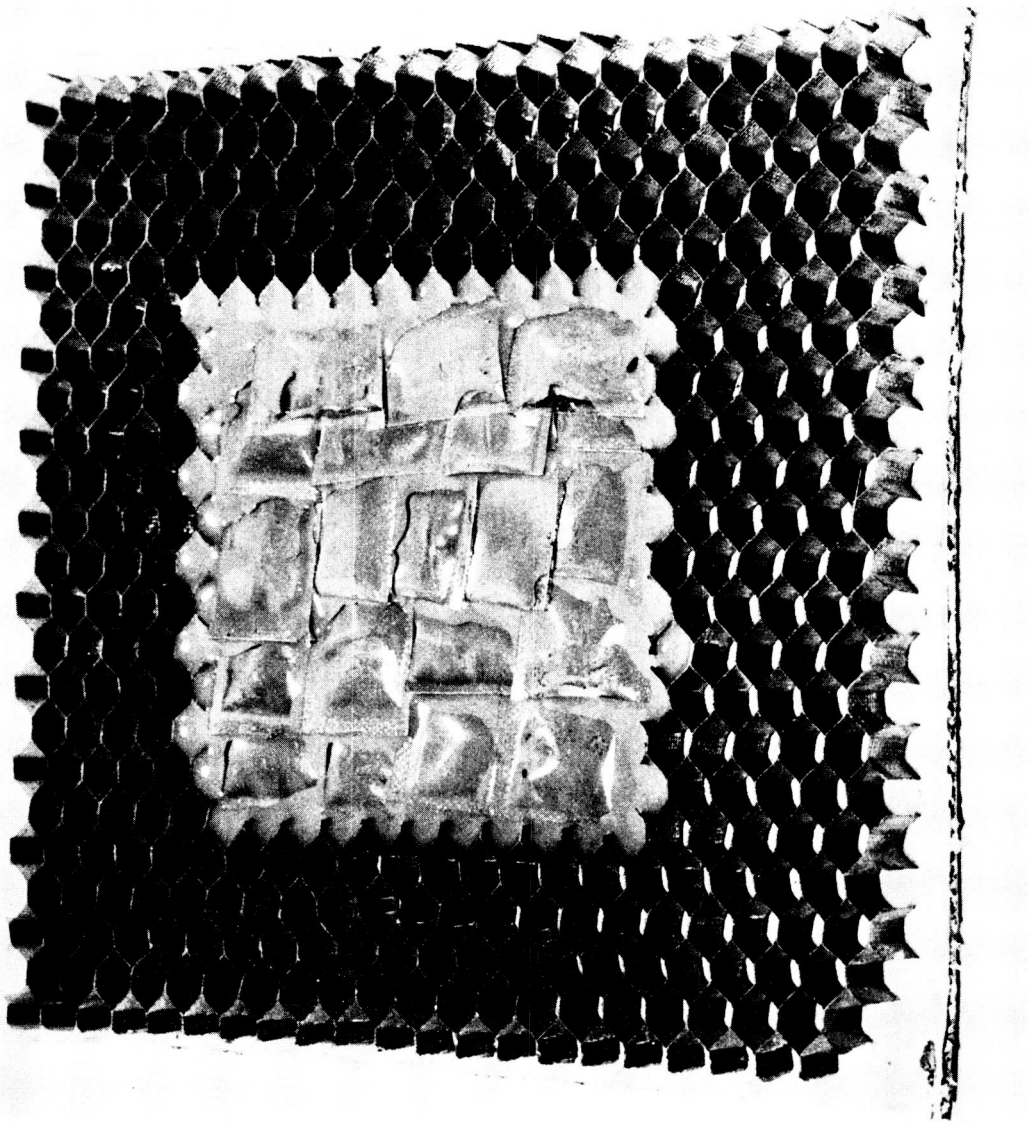

FIGURE 13 CHEMICAL BAG CONCEPT

STRESS-STRAIN:

$$\dot{\varepsilon} = \frac{\dot{\sigma}}{E} + \frac{\sigma}{\eta}$$

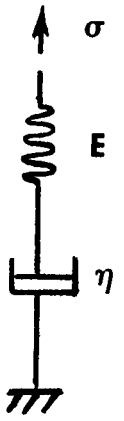

MAXWELL BODY

COMPLEX MODULUS: $E^* = E' + iE''$

$$E' = \left(\frac{\eta}{E}\right) \omega E''$$

STRESS-STRAIN:

$$\sigma = E\varepsilon + \eta\dot{\varepsilon}$$

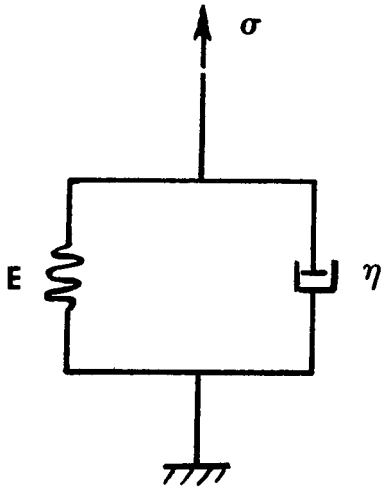

KELVIN BODY

COMPLEX MODULUS: $E^* = E' + iE''$

$$E' = \left(\frac{E}{\eta}\right) \frac{E''}{\omega}$$

FIGURE 14 CLASSICAL VISCOELASTIC BODIES

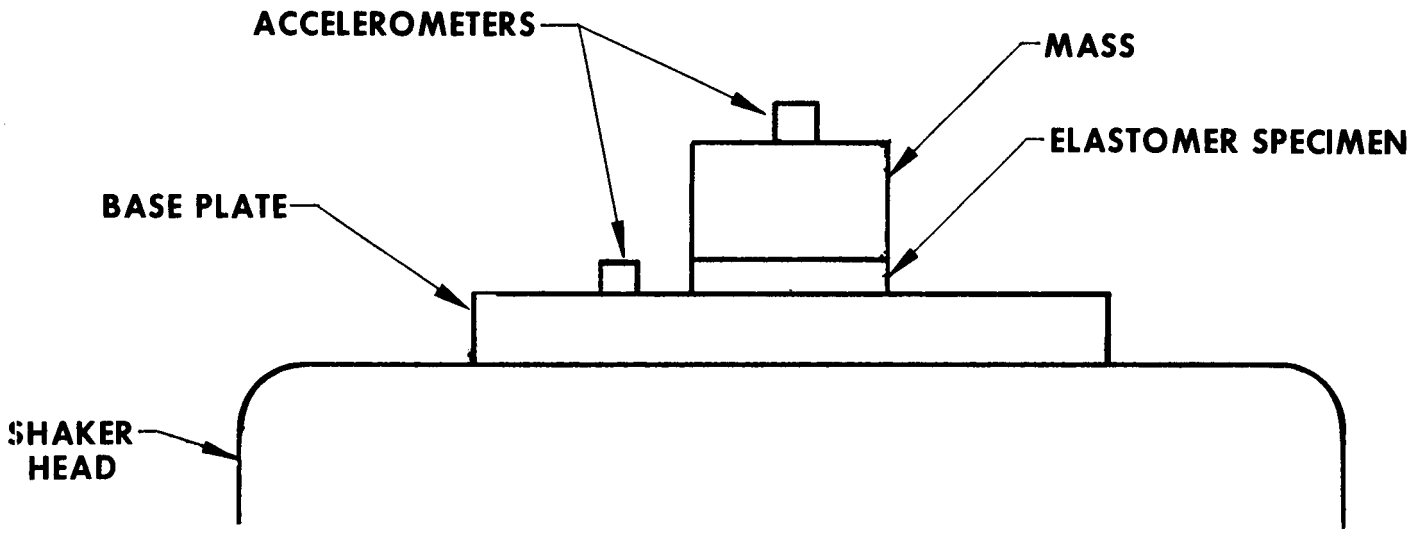

FIGURE 15 SHAKER TEST SETUP

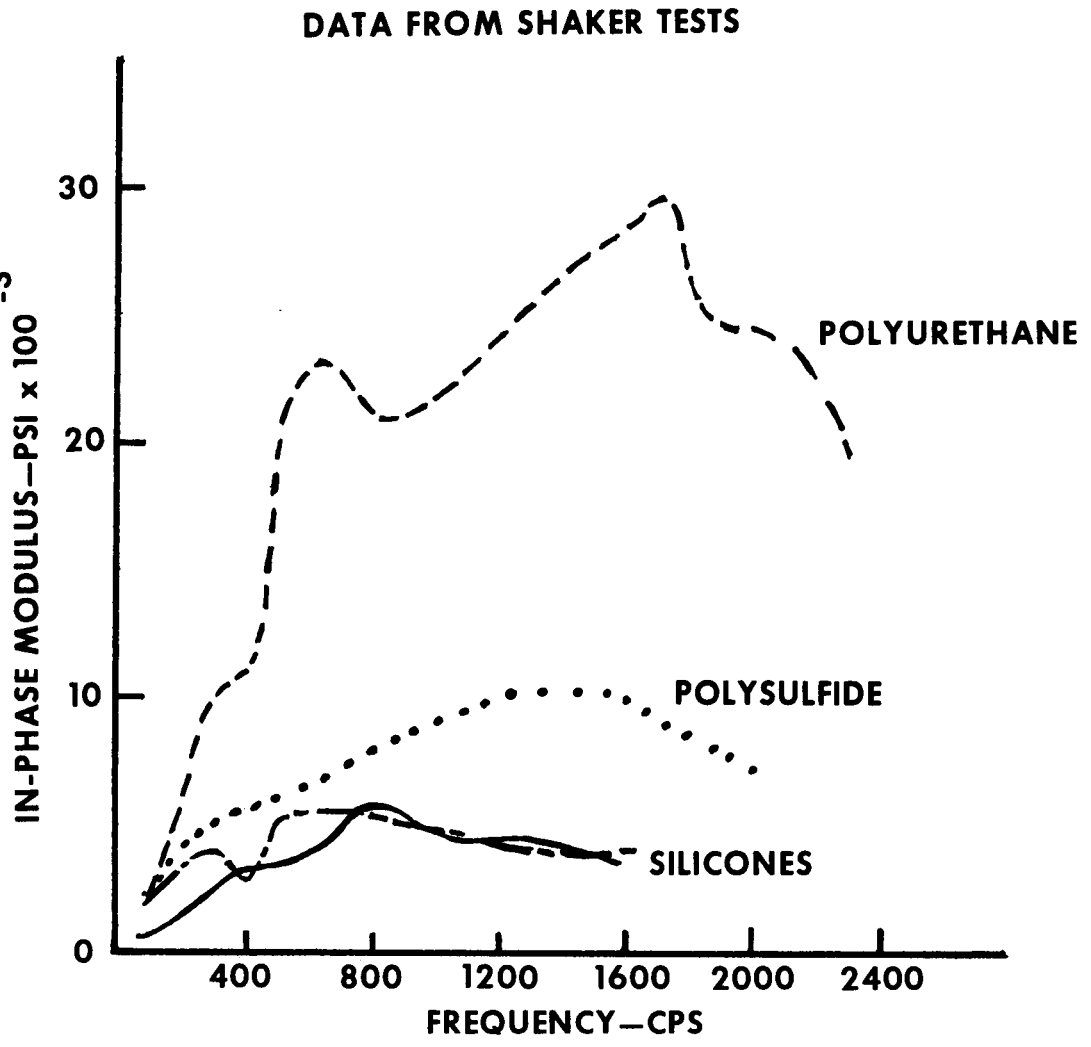

FIGURE 16 IN-PHASE (ELASTIC) MODULUS VS. FREQUENCY

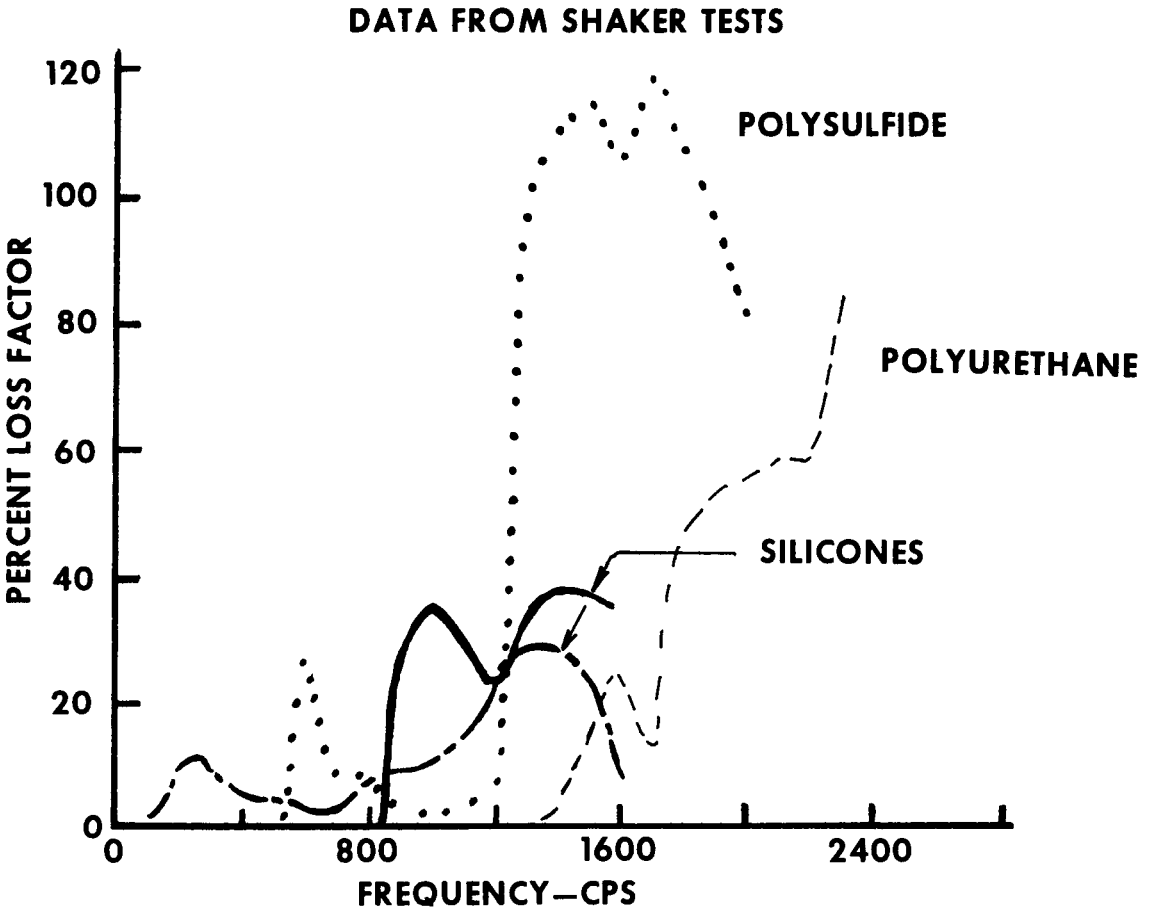

FIGURE 17 LOSS FACTOR VS. FREQUENCY